CELL BIOPHYSICS

Original article

ION HOMEOSTASIS IN THE REGULATION OF INTRACELLULAR pH AND VOLUME OF HUMAN ERYTHROCYTES

O. I. Dotsenko*⍟**, G. V. Taradina**⍟
Vasyl' Stus Donetsk National University, 21 600-richchia Str, Vinnytsia, 21021, Ukraine
*Corresponding author: o.dotsenko@donnu.edu.ua

Background: Cell volume maintenance by regulating the water and ion content is crucial for the survival and functional fullness of human erythrocytes. However, cells are incredibly complex systems with numerous, often competing, reactions occurring simultaneously. Hence, anticipating the overall behavior of the system or acquiring a new understanding of how the subcomponents of the system interact might pose a considerable challenge in the absence of employing mathematical modeling methods.
Objectives: Creation of a mathematical metabolic model of erythrocyte ion homeostasis to study the mechanisms of erythrocyte volume stabilization and intracellular pH in *in vitro* experiments.
Material and Methods: The mathematical model was developed using general approaches to modeling cellular metabolism, which are based on systems of ordinary differential equations describing metabolic reactions, passive and active ion fluxes. The generation of the model and all computations, relying on the model, were executed utilizing the COPASI 4.38 simulation environment. Changes in intracellular pH, Na^+/K^+-ATPase, and Ca^{2+}-ATPase activities of donor erythrocytes incubated in saline solutions in the absence and presence of Ca^{2+} ions were used to test the model.
Results: The kinetic model of erythrocyte ion homeostasis was created. Using realistic parameters of the system changes over time in cell volume, concentrations of metabolites, ions fluxes and transmembrane potential were calculated. The simulation results were used to analyze the reasons for changes in the resistance to acid hemolysis of erythrocytes under the conditions of their incubation in saline solutions of different compositions.
Conclusion: We show that cation homeostasis in erythrocytes is maintained mainly by the active movement of Na^+ and K^+ through Na^+, K^+-ATPase, combined with relatively lower passive permeability through other transport pathways. In the presence of Ca^{2+} ions and the activation of potassium release through Gardos channels, the cell volume is stabilized due to a change in the transmembrane potential and activation of electrodiffusion ion fluxes. The study demonstrated that the reduction in acid resistance of erythrocytes during incubation in a saline solution is associated with a decrease in their cell volume, whereas the increase in acid resistance during incubation in the presence of Ca^{2+} ions is linked to the activation of the Na^+/H^+ exchanger.
KEY WORDS: mathematical metabolic modeling; ion transport; osmotic processes; electrochemical membrane potential; permeant ions; Na^+/K^+-ATPase; Ca^{2+}-ATPase; calmodulin; Band3 protein (AE1); Gardos channels.

The viability and functional completeness of human erythrocytes is determined by their ability to stabilize their volume. The volume of erythrocytes is about 60% of the maximum possible value for a given surface area [1]. This is what determines its ability to strong

deformation, which is necessary to pass through capillaries and transport oxygen [1, 2]. In this regard, the erythrocyte must have special mechanisms to stabilize its volume against changes in the permeability of the cell membrane [3].

It is believed that the erythrocyte volume is completely determined by ion homeostasis [3, 4]. Ion transport is crucial for maintaining ion-water balance and establishing the electrical potential difference between the cell and its surroundings [1]. This is indicated by the fact that the consequence of hereditary and acquired disorders is a change in ion homeostasis and hydration of cells. Overall, the extent of disruption in water and ion content plays a crucial role in determining the severity of hemolytic anemia [4, 5].

Genomic and proteomic studies identify numerous channels, transporters, and regulatory proteins that respond to changes in the osmolality of the environment and are involved in volume control in normal and diseased erythrocytes. The erythrocyte membrane contains a number of carrier proteins that carry out the transport of monovalent cations and anions by the mechanism of facilitated diffusion (Na^+, K^+, $2Cl^-$, K^+, Cl^--cotransport, Na^+/H^+ and HCO_3^-/Cl^- exchange). These systems account for 20% of the total flux of monovalent ions, so it is believed that their main physiological value consists in the regulation of cell volume and control of intracellular pH. It has been shown that swelling of erythrocytes activates K^+, Cl^- cotransport, while a decrease in cell volume leads to activation of Na^+/H^+ exchange and Na^+, K^+, $2Cl^-$-cotransport [6, 7]. Activated by Ca^{2+} ions potassium channels are also involved in autoregulation of erythrocyte volume [8, 9]. Investigating the connection between erythrocyte membrane permeability and cell volume holds significant importance in unraveling the mechanisms that govern the functional integrity and viability of these cells.

Erythrocyte homeostasis encompasses a specific set of vital cellular processes aimed at preserving and repairing cell volume and integrity amid the dynamic alterations induced by physiological stress. [10]. The main participants of the erythrocyte's homeostasis-related processes are a complete set of passive and active membrane transporters, hemoglobin as the main macromolecular colloid osmotic factor, proton and calcium buffer, cellular metabolites affecting fixed negative charges and additional buffering capacity of the cytoplasm of erythrocytes. Cells are incredibly complex systems with numerous, often competing, reactions occurring simultaneously. Therefore, predicting the overall behavior of the system or gaining a new understanding of how the components of the system interact is quite challenging without the use of mathematical modeling methods.

Mathematical models have been instrumental in advancing the understanding of cell volume regulation [11–15]. The models answered many questions that were either very difficult or impossible to answer experimentally, predicted a number of unexpected relationships in cellular metabolism, and helped to understand how cells use certain biochemical processes. Most of them consider the dynamics of changes in cell volume and pH in the process of blood circulation. We are particularly interested in the application of mathematical models for the interpretation of experimental data obtained in in vitro experiments.

The work aimed to create a mathematical metabolic model of erythrocyte ion homeostasis to study the mechanisms of stabilization of erythrocyte volume and intracellular pH in an in vitro experiment. The developed model represents only a subsystem of a much more complex real system, which has already been described by mathematical models [16 – 18]. In this work, we model only ion hemostasis and will not consider the metabolic processes that contribute to its regulation. We demonstrate that this model is sufficient for analyzing the role of ion homeostasis in the regulation of pH and volume in erythrocytes. It enables us to identify the factors contributing to changes in the hemolytic resistance of erythrocytes during their incubation in various saline solutions.

MATHEMATICAL MODEL AND MODELING METHODS

Common approaches to modeling cellular metabolism typically rely on coupled systems of ordinary differential equations (ODEs), where the cell can be considered a well-mixed chemical reactor. Each ODE represents the sum of all rates of change of a single cellular component.

The model describes the dynamic behavior of a suspension of identical erythrocytes in a saline buffer medium. The extracellular space was treated as a well-mixed compartment and the unmixed layers around the cells were not considered. The size of the extracellular compartment was precisely calculated and expressed in μ^3. The physiologically normal volume of erythrocytes was taken as 90 μ^3 [11, 13].

The physical laws limiting the behavior of such a system are the conservation of charge and mass.

The incubation medium electroneutrality of (Na-phosphate buffer, NaCl) is represented as a linear combination of extracellular ion concentrations. Subscripts *in* and *out* denote intracellular and extracellular concentrations, respectively.

$$(Na^+_{out} + K^+_{out} + 2 \cdot Ca^{2+}_{out}) - (Cl^-_{out} + HCO^-_{3out} + 2 \cdot HPO^{2-}_{4out} + H_2PO^-_{4out}) = 0. \quad (1)$$

The ratio between the ion concentrations of the proton-binding buffer:

$$H_2PO^-_{4out} = \frac{H^+_{out} \cdot HPO^{2-}_{4out}}{6.2 \cdot 10^{-8}}. \quad (2)$$

The electroneutrality of the intracellular medium was described by the equation:

$$(Na^+_{in} + K^+_{in} + 2 \cdot Ca^{2+}_{in} + 2 \cdot Mg^{2+}_{in} + H^+_{in}) - (Cl^-_{in} + HCO^-_{3in} + 2HPO^{2-}_{4in} + H_2PO^-_{4in} +$$
$$+ z(Hb) \cdot Hb + z(2,3BPG) \cdot 2,3BPG = 0 \quad , \quad (3)$$

$z(Hb)$ — the total charge on the hemoglobin molecule, represented by the Cass-Dahlmark equation [12]

$$z(Hb) = a \cdot (pH_{in} - pI) \quad , \quad (4)$$

a corresponds to the linear segment of the proton titration curve of hemoglobin in intact erythrocytes [13], pI — pH at the isoelectric point of hemoglobin. Hb — total hemoglobin concentration.

$$z(2,3BPG) = -5 + \frac{10^{pK_1 - pH_{in}} + 2 \cdot 10^{2 \cdot (pK_2 - pH_{in})}}{1 + 10^{pK_1 - pH_{in}} + 2 \cdot 10^{2 \cdot (pK_2 - pH_{in})}} \quad , \quad (5)$$

$pK_1 = 7.31, pK_2 = 6.2$.

The osmolarity of the external and intracellular environment was described by equations (6), (7):

$$Os_{out} = Na^+_{out} + K^+_{out} + Ca^{2+}_{out} + Cl^-_{out} + HCO^-_{3out} + HPO^{2-}_{4out} + H_2PO^-_{4out} \quad (6)$$

$$Os_{in} = Na^+_{in} + K^+_{in} + Ca^{2+}_{in} + Mg^{2+}_{in} + Cl^-_{in} + HCO^-_{3in} + H^+_{in} + HPO^{2-}_{4in} + H_2PO^-_{4in} +$$
$$+ A + f(Hb) \cdot Hb + 2,3BPG + N \quad , \quad (7)$$

$f(Hb)$ — osmotic coefficient of hemoglobin, represented by the equation [12]:

$$f(Hb) = 1 + 0.0645 \cdot Hb/\alpha + 0.0258 \cdot (Hb/\alpha)^2 , \; \alpha = \frac{V}{V_0}, \quad (8),$$

A — the intracellular osmolytes content (20 mM), *N* — total concentration of cellular nucleotides.

The processes involved in the model are shown in Table 1 and Figure 1

The dissolution of CO_2 and O_2 in a buffered extracellular solution, the process of CO_2 hydration was described as in [16] under the experimental conditions: T=293 K, PO$_2$=160 mmHg, PCO$_2$ = 0.3 mmHg.

The Jacobs-Stewart cycle is described in detail by us in [16]. In this model, the kinetic equation of the HCO_3^- / Cl^- exchange involving AE1 was adjusted, considering the data on the activation of the exchanger by intracellular Ca^{2+} [19]

$$v = \left(k_1 \cdot HCO_{3\ out}^- - \frac{k_2 \cdot \left(1 + 10^{pH_{in} - pK_a}\right)}{1 + \dfrac{10^{pH_{in} - pK_a}}{r}} HCO_{3\ in}^- \right) \cdot \left(1 + \frac{Ca_{in}^{2+}}{Ka}\right), \qquad (9)$$

$k_1 = k_2 = 6,9 \cdot 10^{-6} c^{-1}$, $pKa = 6.3$, r — Donnan's ratio, $Ka = 10\,nM$ (activation constant, $K_{1/2}$).

The transport of CO_2, the hydration of CO_2 with the participation of carbonic anhydrase (CA), the buffering processes of H^+ and CO_2 by hemoglobin have been described in detail by us previously [16] and are used without modification in this model.
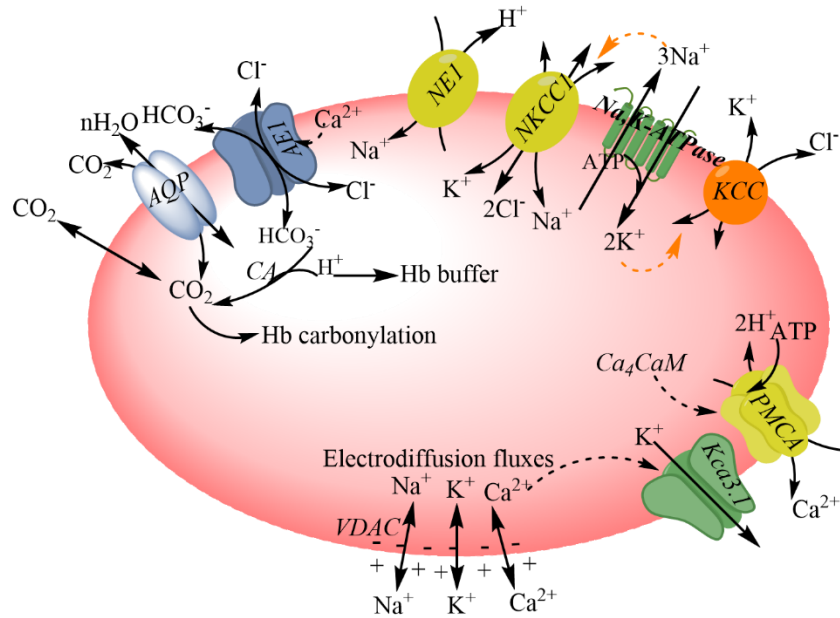

Fig. 1. Scheme of ion transport pathways of the human erythrocyte used in the model. Gradient-driven transport pathways include AE1 (the anion exchange protein 1, band 3), NKCC1 (Na⁺, K⁺, 2Cl⁻-cotransporter 1); KCC (K⁺, Cl⁻-cotransporters), NHE1 (the sodium/hydrogen exchanger 1), VDAC — voltage-regulated ions channels. Membrane channels are the aquaporins (AQP1), K_Ca3.1 (KCNN4, the Gardos channel, a calcium-activated potassium channel). Active transporters are the Ca²⁺-ATPase (PMCA), sodium-potassium ATPase. CA — Carbonic Anhydrase.

Transport of ions

There are several types of channels and carriers that carry out passive transport of ions in the erythrocyte membrane. These are Na⁺, K⁺, 2Cl⁻-cotransport K⁺, Cl⁻-cotransport, Na⁺/H⁺-exchanger, HCO₃⁻/Cl⁻-exchanger.

K⁺, Cl⁻- and Na⁺, K⁺, 2Cl⁻-cotransport was described as in works [14, 15]:

$$J_{K^+,Cl^-} = k_{K,Cl} \cdot (K_{out}^+ \cdot Cl_{out}^- - K_{in}^+ \cdot Cl_{in}^-), \qquad (10)$$

$k_{K,Cl}$ — the transport rate constant, $k_{K,Cl} = 4.56 \cdot 10^{-3} M^{-1} \cdot s^{-1}$.

$$J_{K^+,Na^+,2Cl^-} = k_{K,Na,2Cl} \cdot (K_{out}^+ \cdot Na_{out}^+ \cdot Cl_{out}^{-2} - K_{in}^+ \cdot Na_{in}^+ \cdot Cl_{in}^{-2}), \qquad (11)$$

$k_{K,Na,2Cl}$ — the transport rate constant, $k = 4.37 \cdot 10^{-4} M^{-3} \cdot s^{-1}$.

The rate of transport through the Na^+/H^+-exchanger was described by kinetics, according to [20, 21]:

$$J_{Na^+/H^+} = (7.2 - pH_{in}) \cdot \frac{V \cdot H_{in}^{+n}}{K + H_{in}^{+n}},$$ (12)

$V = 1.78 \cdot 10^{-5} M / s, \ K = 0.285 \, mM, \ n = 1.85.$

Table 1. Reactions involved in the model (arrow type, $\rightarrow$ or $\leftrightarrow$, indicates whether the reaction is considered irreversible or reversible in the analysis)

N	Reactions	Enzymes	Effectors
	Medium		
1	$CO_{2out} + H_2O \rightleftarrows HCO_{3\,out}^- + H_{out}^+$	Non enzymatic reaction	P_{CO_2}, T
2	$HPO_{4out}^{2-} + H_{out}^+ \rightleftarrows H_2PO_{4out}^-$	Non enzymatic reaction	
	Cell		
	Jacobs-Stewart cycle		
3	$CO_{2in} + H_2O \rightleftarrows HCO_{3in}^- + H_{in}^+$	CA	
4	$CO_{2in} \rightleftarrows CO_{2out}$	Transport	
5	$HCO_{3out}^- + Cl_{in}^- \rightleftarrows HCO_{3\,in}^- + Cl_{out}^-$	AE1 transport	Ca_{in}^{2+}
	Ion's transport		
	Electrodiffusional flux		
6	$Na_{out}^+ \rightleftarrows Na_{in}^+$	VDAC transport	E
7	$K_{in}^+ \rightleftarrows K_{out}^+$	VDAC Transport	E
8	$K_{in}^+ \rightleftarrows K_{out}^+$	Gardos channel (KCNN4)	Ca_{in}^{2+}, E
9	$Ca_{out}^{2+} \rightleftarrows Ca_{in}^{2+}$	VDAC transport	E
	Electroneutral transport		
10	$K_{out}^+ + Cl_{out}^- \rightleftarrows K_{in}^+ + Cl_{in}^-$	K^+Cl^- cotransporter (KCC)	
11	$K_{out}^+ + Na_{out}^+ + 2Cl_{out}^- \rightleftarrows K_{in}^+ + Na_{in}^+ + Cl_{in}^-$	$Na^+K^+2Cl^-$ cotransporter (NKCC1)	
12	$Na_{out}^+ + H_{in}^+ \rightleftarrows Na_{in}^+ + H_{out}^+$	Na^+/H^+ exchanger (NE1)	pH, Ca_{in}^{2+}
	ATPase		
13	$2K_{out}^+ + 3Na_{in}^{++} \rightleftarrows 2 K_{in}^+ + 3Na_{out}^+$	$Na^+, K^+ - ATPase$	ATP
14	$Ca_{in}^{2+} + 2H_{out}^+ \rightarrow Ca_{out}^{2+} + 2H_{in}^+$	$Ca^{2+} - ATPase$ (PMCA1)	ATP, Ca_4CaM
	Hb-buffer's capacity		
15	$deoxyHb + H_{in}^+ \rightleftarrows HdeoxyHb$		
16	$oxyHb + H_{in}^+ \rightleftarrows HoxyHb$		
17	$deoxyHb + CO_2 \rightleftarrows carbHb + H_{in}^+$		

O. I. Dotsenko, G. V. Taradina

N	Reactions	Enzymes	Effectors
18	$oxyHb + CO_2 \rightleftarrows carbHb + H_{in}^+$		
	Binding of metabolites to hemoglobin		
19	$deoxyHb + 23BPG \rightleftarrows deoxyHb23BPG$		
20	$deoxyHb + ATP \rightleftarrows deoxyHbATP$		
21	$deoxyHb + ADP \rightleftarrows deoxyHbADP$		
22	$deoxyHb + MgATP \rightleftarrows deoxyHbMgATP$		
23	$oxyHb + 23BPG \rightleftarrows oxyHb23BPG$		
24	$oxyHb + ATP \rightleftarrows oxyHbATP$		
25	$oxyHb + ADP \rightleftarrows oxyHbADP$		
26	$oxyHb + MgATP \rightleftarrows oxyHbMgATP$		
	Ca^{2+}, Mg^{2+} interactions		
27	$Mg_{in}^{2+} + ATP \rightleftarrows MgATP$		pH
28	$Ca_{in}^{2+} + ATP \rightleftarrows CaATP$		pH
29	$Ca_{in}^{2+} + 23BPG \rightleftarrows Ca23BPG$		pH
30	$MgADP + ADP \rightleftarrows MgATP + AMP$	AK	pH
	Ca^{2+}-calmodulin interactions		
31	$CaM + 2Ca_{in}^{2+} \rightleftarrows Ca_2CaM$		pH
32	$Ca_2CaM + 2Ca_{in}^{2+} \rightleftarrows Ca_4CaM$		pH

The electrodiffusion flux Na$^+$, K$^+$, Ca^{2+} was described by the Goldman equation:

$$J_j = -\frac{P_j \cdot z \cdot E \cdot F}{R \cdot T} \frac{C_j^{out} - C_j^{in} \cdot e^{\frac{z \cdot E \cdot F}{R \cdot T}}}{1 - e^{\frac{z \cdot E \cdot F}{R \cdot T}}}, \tag{13}$$

P_j — the ion permeabilities. $P_{Na^+} = 3.38 \cdot 10^{-6}\, s^{-1}$, $P_{K^+} = 3.44 \cdot 10^{-6}\, s^{-1}$ [11]. In the absence of Ca^{2+} in the incubation medium $P_{Ca^{2+}} = 2.11 \cdot 10^{-7}\, s^{-1}$, in the presence of Ca^{2+} $P_{Ca^{2+}}$ was calculated as function of Ca^{2+} [14]:

$$P_{Ca^{2+}} = \left(\frac{Ca_{in}^{2+}}{0.04 + Ca_{in}^{2+}} \right) \cdot \left(\frac{Ca_{out}^{2+}}{0.8 + Ca_{out}^{2+}} \right). \tag{14}$$

The K$^+$ permeability through the Gardos channel was calculated as [11]:

$$P_{K^+\_Gardos} = P \cdot \left(\frac{Ca^{2+}}{K + Ca^{2+}} \right)^4, \tag{15}$$

$P = 4.72 \cdot 10^{-4}\, s^{-1}$, $K = 0.25\, \mu M$ [11].

E — the transmembrane potential was calculated as:

$$E = -\frac{R \cdot T}{F} \ln \frac{P_{K^+} \cdot K_{in}^+ + P_{Na^+} \cdot Na_{in}^+ + P_{Cl^-} \cdot Cl_{out}^-}{P_{K^+} \cdot K_{out}^+ + P_{Na^+} \cdot Na_{out}^+ + P_{Cl^-} \cdot Cl_{in}^-}, \tag{16}$$

in the presence of Ca^{2+} in the incubation medium

$$E = -\frac{R \cdot T}{F} \ln \frac{(P_{K^+} + P_{K^+Gardos}) \cdot K_{in}^+ + P_{Na^+} \cdot Na_{in}^+ + P_{Cl^-} \cdot Cl_{out}^-}{(P_{K^+} + P_{K^+Gardos}) \cdot K_{out}^+ + P_{Na^+} \cdot Na_{out}^+ + P_{Cl^-} \cdot Cl_{in}^-}, \tag{17}$$

F — the Faraday constant; R — universal gas constant; T — absolute temperature; P_{K^+}, P_{Na^+}, P_{Cl^-} — erythrocyte membrane passive permeabilities of the K^+, Na^+, Cl^- respectively, K^+, Na^+, Cl^- — the ion concentrations in the extracellular environment and in the cell.

Active transport of ions

Ca^{2+}-ATPase transports Ca^{2+} independently and irreversibly, and when it binds to the Ca-calmodulin complex, it transports Ca^{2+} with a much higher affinity and rate of exchange [22]. It is known that the activity of the Ca^{2+}-ATPase is depended on the concentration of ATP [23] and is inhibited by high concentrations of intracellular calcium [24]. The equation for the rate of active Ca^{2+} transport given in [23] was modified by us as follows:

$$v = \frac{V \cdot \left(Ca^{2+}\right)^n ATP}{\left(K + Ca^{2+}\right)^n \left(1 + \dfrac{Ca^{2+}}{K_I}\right)} \cdot \left(1 + \frac{Ca_4CaM}{K_a}\right), \tag{18}$$

$V = 0.03\,M/s$, $K = 1.1\,\mu M$ [23], $K_a = 1\,\mu M$, $K_I = 0.6\,\mu M$ (was set during simulation). n — the cooperativity factor that characterize Ca^{2+} activation of the enzyme ($n = 2$ in the absence of Ca^{2+} ions, $n = 4$ in the presence of Ca^{2+} in the incubation medium [11, 14]).

Na$^+$, K$^+$-ATPase activity was described by using the kinetic equation given in [18], taking into account the inactivation of the enzyme by Ca^{2+} ions [25].

$$v = \frac{\left(\dfrac{ATP}{ATP + K_m}\right) \cdot \left(\dfrac{V_m}{2}\right) \cdot \left(\left(K_{out}^+\right)^2 + \dfrac{z \cdot B_2 \cdot K_{out}^+}{2}\right)}{Pump \cdot \left(1 + \dfrac{Ca^{2+}}{K_I}\right)}, \tag{19}$$

$$Pump = B_1 \cdot B_2 + 2B_2 \cdot K_{out}^+ + \left(K_{out}^+\right)^2 + \left(\frac{B_3}{Na_{in}^+} + 1\right)^3 \cdot (B_1 \cdot B_2 \cdot k_1 \cdot k_2 + k_1 \cdot k_3 \left(K_{out}^+\right)^2 + z \cdot B_2 \cdot K_{out}^+),$$

$V_m = 0.452\,mM/s$, $B_1 = 6.17 \cdot 10^{-8}\,M$, $B_2 = 1.33 \cdot 10^{-5}\,M$ (was adjusted during simulation), values of other parameters of the equation are taken from [18] without changes. $K_I = 0.398\,\mu M$ (Na$^+$, K$^+$-ATPase inhibition constant ($K_{1/2}$) by Ca^{2+} ions).

The kinetics of 2,3BPG, ATP, ADP, Mg-ATP binding with oxy- and deoxyhemoglobin, Mg^{2+} and Ca^{2+} binding with ATP and 2,3BPG are described in works [17, 18], and the parameters and kinetic equations of these reactions are applied in the model without modification.
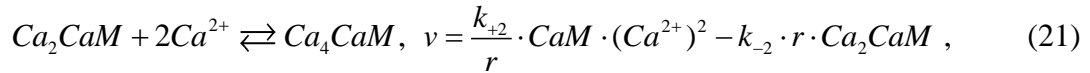
Interaction of Ca^{2+} with calmodulin

The interaction of calcium with calmodulin was described by mass action kinetics. The rate constants given in [26] were normalized by the parameter r (cooperativity factor), which considers the dependence of Ca^{2+} binding with calmodulin on pH. Experimental dependences of r on pH for two types of Ca^{2+} binding centers with calmodulin are given in [27]. The regression dependence of r on pH was obtained by us and applied in the model

$$CaM + 2Ca^{2+} \rightleftarrows Ca_2CaM, \quad v = \frac{k_{+1}}{r} \cdot CaM \cdot (Ca^{2+})^2 - k_{-1} \cdot r \cdot Ca_2CaM, \tag{20}$$

$k_{+1} = 2.669 \cdot 10^{12}\,M^{-2} \cdot s^{-1}$, $k_{-1} = 2.682\,s^{-1}$ [26],

$r = -0.0403\,pH^3 + 1.0126\,pH^2 - 8.5561\,pH + 25.966$.

$$Ca_2CaM + 2Ca^{2+} \rightleftarrows Ca_4CaM, \quad v = \frac{k_{+2}}{r} \cdot CaM \cdot (Ca^{2+})^2 - k_{-2} \cdot r \cdot Ca_2CaM, \quad (21)$$

$k_{+2} = 1.704 \cdot 10^{14} M^{-2} \cdot s^{-1}$, $k_{-2} = 1.551 s^{-1}$ [26].

The change in intracellular ATP content was specified as a time dependence obtained by a result of approximating experimental data [28] with the 4th-order regression equation.

The kinetics of adenylate kinase (AK) was described by the equation used in the model of human erythrocyte metabolism [17], which is in the BioModels Database (www.ebi.ac.uk/biomodels/MODEL5950552398#Files). The flux through this reaction is represented as *pH*-dependent kinetics.

The volume of the erythrocyte is determined by the balance of osmotic values inside (Os_{in}) and outside (Os_{out}) the cell. The volume of the cell was described by the equation:

$$\frac{dV}{dt} = J_w = P_w \cdot R \cdot T(Os_{in} - Os_{out}),$$

$$P_w = 6.02 \cdot 10^{-6} \mu / s, \quad (22)$$

P_w — permeability coefficient for water.

The developed model is a system of differential and algebraic equations that describes changes in ion concentrations, cell's volume and transmembrane potential, fluxes through all regulatory elements depending on ion permeability, kinetic parameters of enzymatic and non-enzymatic reactions, concentrations of impermeable ions and osmolarity of the extracellular medium.

Model creation and all numerical calculations based on the model were performed using the COPASI 4.38 simulation environment.

The determination of numerical values for certain kinetic parameters within the reaction rate equation, along with the initial values of intracellular CO_2 and HCO_3^-, involved a search for optimal conditions that yielded the best agreement between the experimental and calculated dependencies of *pH_in* values. This process was carried out during the solution of the systems of equations incorporated in the model [16].

The objective function has the form:

$$O(p) = \sum_j \sum_k \left(pH_{k,j} - pH_{k,j}(p) \right)^2, \quad (23)$$

$pH_{k,j}$ the experimental value of *pH_in* when measuring j in experiment k and the corresponding calculated value $pH_{k,j}(p)$, p — vector of estimated parameters during modeling [16].

In the work, the search for some parameters of the model is performed using the Evolutionary Programming method. The result of searching for parameters is a set of kinetic parameters characterizing the speed of each process in the system.

Using of the model, families of kinetic curves describing changes in concentrations of substrates and products, fluxes of relevant processes over time for the studied system were obtained.

EXPERIMENTAL STUDIES

The experimental protocol in this study adheres to the principles of biological ethics and has received approval from the Local Ethics Committee of the Vasyl Stus Donetsk National University, Faculty of Chemistry, Biology and Biotechnology (Vinnytsia, Ukraine) [30–32].

The experiments employed freshly obtained blood from donors within a similar age group and of the same gender [30]. Erythrocytes were separated from plasma by

centrifugation and washed three times with Na-phosphate buffer (0.015 M, pH 7.4) containing 0.15 M NaCl (medium 1) [31, 32]. The total hemoglobin content in the acquired packed erythrocytes was assessed through the standardized cyanmethemoglobin method.

Erythrocytes were incubated for 3 hours at a temperature of 20°C:

- in medium 1,

- in medium 1 with the addition of calcium chloride in the amount of 2 mM (simulation of changes in calcium hemostasis). During the experiment, the investigated system was in contact with ambient air.

The hemoglobin content in the studied suspensions was at the level of 3±0.18 mg/ml.

Determination of intracellular pH value

pH_{in} levels were examined in hemolysates of erythrocytes before the initiation of the experiment and subsequently every 20 minutes during the incubation in a buffer solution, with and without Ca^{2+} ions. After certain time intervals, 2 ml of erythrocyte suspension was subjected to centrifugation at 3000 rpm for 1 min. The supernatant was carefully removed; the cells were lysed by adding 1 ml of deionized water. The pH value was measured using a laboratory ionomer using a combined electrode (ESK-10614/7) [16, 18].

The study of the dynamics of acid hemolysis

The study of the dynamics of acid hemolysis was carried out as in [33]. Every 20 min of cell incubation, 2 ml of the suspension was taken. Changes in the optical density of the erythrocyte suspension after adding an equal amount of hemolytic agent (4 mM HCl) were recorded at a wavelength of 650 nm with a time interval of 1 s in automatic mode. As the main kinetic parameters characterizing the structural properties of erythrocytes, the kinetic parameters of hemolysis were used: lag phase time (t_{lag}) and the rate constant of hemoglobin release from the cell (k). A sample without incubation was used as a control.

Study of the activities of Na^+,K^+-ATPase and Ca^{2+}-ATPase

Enzymes activities were determined in the hemolysate of cells, which was added to the medium containing ATP. The composition of the medium for determining Na^+, K^+-ATPase: 3 mM $MgCl_2$, 125 mM NaCl, 25 mM KCl, 3 mM ATP, 0.5 mM EDTA, 50 mM Tris-HCl, pH 7.4, ±0.5 mM ouabain [34]. The composition of the medium for determining Ca^{2+}-ATPase: 3 mM $MgCl_2$, 100 mM KCl, 3 mM ATP, 0.06 mM EDTA, 50 mM Tris-HCl, pH 7.4, ±0.9 mM $CaCl_2$.

Samples were incubated for 15 minutes. The reaction was stopped by adding 0.1 ml of cold trichloroacetic acid. A color reaction with ammonium molybdenum was used to determine the content of inorganic phosphate (Pn) [28]. The optical density of the solutions was recorded spectrophotometrically at a wavelength of 590 nm in cuvettes with a thickness of 1 cm. The *pH* value was determined using a calibration graph constructed for a standard solution of the exact concentration. The activity of Na^+,K^+-ATPase was evaluated by the difference in the accumulation of Pn in the medium without ouabain and with ouabain. Ca^{2+}-ATPase activity according to the difference in Pn accumulation in Ca^{2+}-containing and Ca^{2+}-free media. The activity of marker enzymes was expressed in μM Pn, formed for 1 minute, related to the amount of protein (Hb) in the sample (μM/min·mg Hb).

All experiments were carried out in triplicate. Experimental data were analyzed in the Statistica 8.0 program (StatSoft Inc., USA). Experimental data are presented as *x*±SE (*x* is the mean, SE is the standard error of mean) [16]. The regression dependence of the studied parameters on the time of the experiment was constructed using the Distance Weighted Least Squares function, *p*=0.25.

O. I. Dotsenko, G. V. Taradina

RESULTS AND DISCUSSION

pH regulation in erythrocytes (a comparison between experiment and theory)

Changes in intracellular pH (pH_{in}) during incubation of erythrocytes in the absence and presence of Ca^{2+} in the medium are shown in Figure 2 a, b. The calculations (Figure 2 a, b, solid lines) show that, under the chosen parameters, the model accurately describes the obtained experimental data, which indicates its adequacy and the possibility of its application to the analysis of ion homeostasis and prediction.
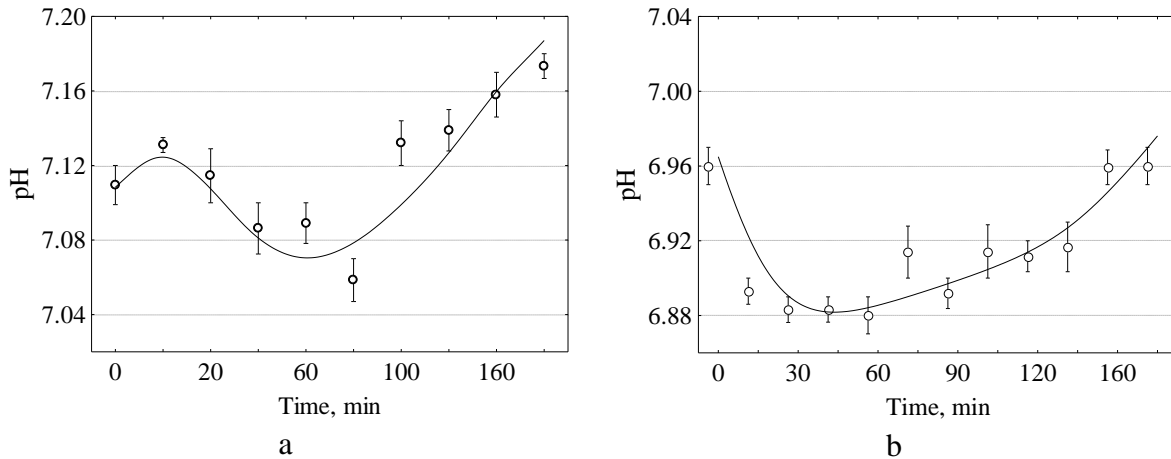

Fig. 2. Changes in pH in erythrocytes during their incubation in Na-phosphate buffer medium (0.015 M, pH 7.4) containing 0.15 M NaCl without Ca^{2+} (a), in the same medium containing 2 mM Ca^{2+} (b). Each point is represented as x ± m for n = 5. The solid line is the calculated dependence of pH in obtained by the model.

As we have shown previously [16], the main contribution to pH regulation is made by the Jacobs-Stewart cycle (reactions 3–5, Table 1) and the combined processes of H^+ buffering and carbonylation (reactions 15–18, Table 1). The intracellular and extracellular activity of HCO_3^- is related to the corresponding activity of H^+ through hydration/dehydration reactions between HCO_3^- and carbon dioxide. This reaction is catalyzed by the enzyme carbonic anhydrase in the intracellular compartment [35] and proceeds at an uncatalyzed rate in the extracellular compartment (reaction 1), which makes extracellular reactions limiting for acid balance across the erythrocyte membrane [36].

Calculation of the flux through the HCO₃⁻/Cl⁻ anion exchanger

The calculated flux through the HCO_3^-/Cl^- anion exchanger (AE1, CDB3) is shown in Fig. 3 a. During incubation in an environment without Ca^{2+}, the outflux of Cl^- from the cell gradually slows down (Fig. 6 a) and the reverse process of exchanging intracellular HCO_3^- for extracellular Cl^- becomes dominant. It is known that the presence of Ca^{2+} in the medium activates AE1 [19]. The mechanism of AE1 activation has not been precisely investigated. It is believed that AE1 can be activated either during the direct interaction of Ca^{2+} with AE1 or with the participation of intracellular enzymes sensitive to an increase in the content of Ca^{2+} in the cell. It is known that CDB3 serves as a binding site for phosphatases and kinases that regulate protein activity [19, 37]. An intracellular rise in Ca^{2+} causes phosphor tyrosine phosphatase to dissociate from CDB3, leaving a tyrosine kinase that activates CDB3.

AE1 (CDB3) activation is modeled by us using Michaelis–Menten kinetics, which formally describes the stimulated activation of CDB3. The activation constant ($K_a = 1\,\mu M$) was found by us in the process of parameters optimization. Based on the simulation results, as intracellular Ca^{2+} levels rise, the flux through AE1 rapidly undergoes a sign change (with the

reverse flux direction prevailing, as indicated in Table 1) and attains a steady-state level 18 times higher than the flux of HCO_3^- through the carrier in the absence of Ca^{2+} in the incubation medium.
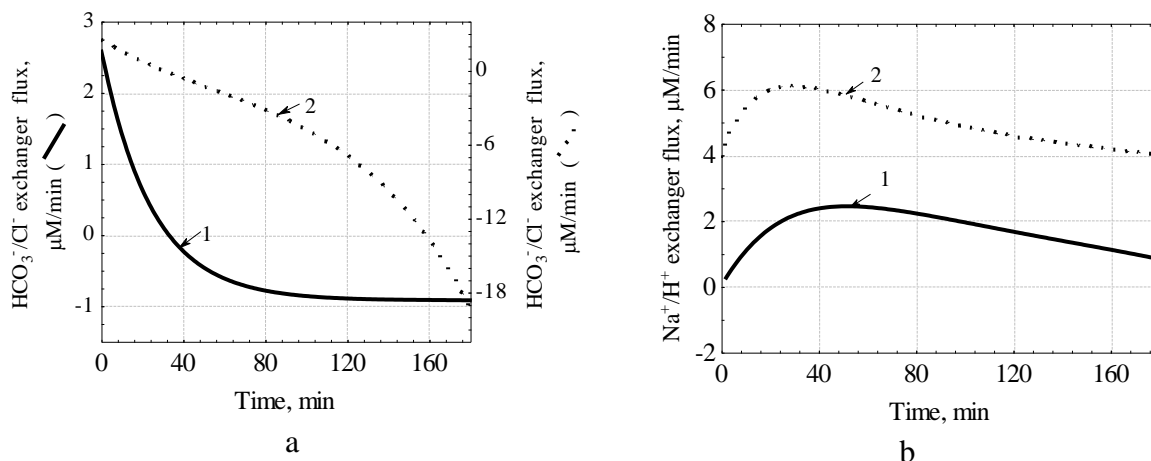

Fig. 3. Fluxes through an HCO_3^-/Cl^- anionic exchanger (a) and Na^+/H^+ exchanger (b) in the absence (1) and presence of Ca^{2+} (2) in the incubation medium. Dependencies obtained during mathematical modeling.

The present model incorporates the Na^+/H^+ transport system, a shared feature among eukaryotic cells, as a regulatory element for intracellular *pH* and volume control in erythrocytes. The contribution of this carrier has not been considered in existing models. The activity of the Na^+/H^+ exchanger in human erythrocytes is very low [21]. It is believed that the expression of this transporter in mature anucleated erythrocytes may be a remnant of its activity in progenitor stem cells, which at later stages of differentiation receive hemoglobin and an anion exchanger [21] to transport H^+ from the tissue to the lungs. However, it was shown [20] that an increase in cytosolic calcium, a decrease in intracellular pH, and osmotic compression of cells stimulate the influx of Na through this transporter. The sodium gradient across the erythrocyte membrane contributes to the general outflux of protons, Na^+/H^+ exchange creates opportunities to increase intracellular pH [38]. Na^+/H^+ exchange causes a net influx of Na^+ and efflux of H^+, displacing H+ from electrochemical equilibrium within the first minutes of activation. This is possible, even though anion exchange is functional because the rate of Na^+/H^+ exchange approaches the rate of extracellular uncatalyzed hydration/dehydration reactions between HCO_3^- and carbon dioxide. Thus, a large number of protons can be extruded through the Na^+/H^+ exchanger and accumulate in the extracellular compartment before the carbonic acid formed from the accumulated H^+ and HCO_3^- is largely dehydrated to carbon dioxide [35].

The flux through the Na^+/H^+ exchanger of erythrocytes incubated in the absence and presence of Ca^{2+} ions is shown in Figure 3 b. In the presence of Ca^{2+}, the intracellular *pH* is lower (Fig. 2 b), so the flux through the Na^+/H^+ exchanger increases. The inverse correlation of the flux through Na^+/H^+ with intracellular pH shows its contribution to the regulation of the latter.

Na^+, K^+- and Ca^{2+}-ATPases

To verify the simulation results, we obtained experimental dependences of Na^+, K^+ and Ca^{2+}-ATPase activities. Fluxes through these enzymes obtained by model (a) and experiment (b) are shown in Figures 4 and 5. Despite the fact that these indicators have different units of measurement (the flux is determined by the kinetic equation of the model, and the activity is

the change in the concentration of the substrate per unit of time), there is much in common in the nature of the change of these indicators.

According to modern views, the human erythrocyte maintains its volume due to the unbalanced distribution of ions created by the transporter Na^+K^+-ATPase between the intracellular compartment and the extracellular environment [1, 23], if changes in the permeability of the cell membrane are relatively small.

The kinetic behavior of Na^+K^+-ATPase is very complex, and has been studied in detail, and many rate equations describing this behavior are proposed in the literature. In the model, we use the kinetic rate equation [18], that considers additional regulation of Na^+K^+-ATPase due to changes in ATP concentration, which are responsible for changes in the adenylate pool. The value of the adenylate pool depends on the ratio of ATP to AMP, which, in turn, depends on the rate of ATP consumption by Na^+K^+-ATPase [1, 23]. The importance of ATP for Na^+K^+- and Ca^{2+}-ATPase functioning is indicated by the fact that ATP is located in a structurally isolated compartment formed by proteins of the cytoskeleton of erythrocytes, which is the main source of the latter for both enzymes [39]. As shown [23], this regulation provides a good stabilization of intracellular concentrations of ions and, accordingly, the volume of erythrocytes.

We tried to model the changes in the adenylate pool with reactions 27–30 (Table 1), however, using only the adenylate kinase reaction (reaction 28, Table 1) turned out to be insufficient, since the ATP content is regulated by many processes. Previously, we investigated in detail the changes in ATP content in erythrocytes incubated in medium 1 without glucose [28]. To reproduce the similar nature of changes in fluxes through Na^+K^+-ATPase with experimental data, in the model we set the dependence of the change in ATP concentration on the incubation time, which was obtained for the experimental data.
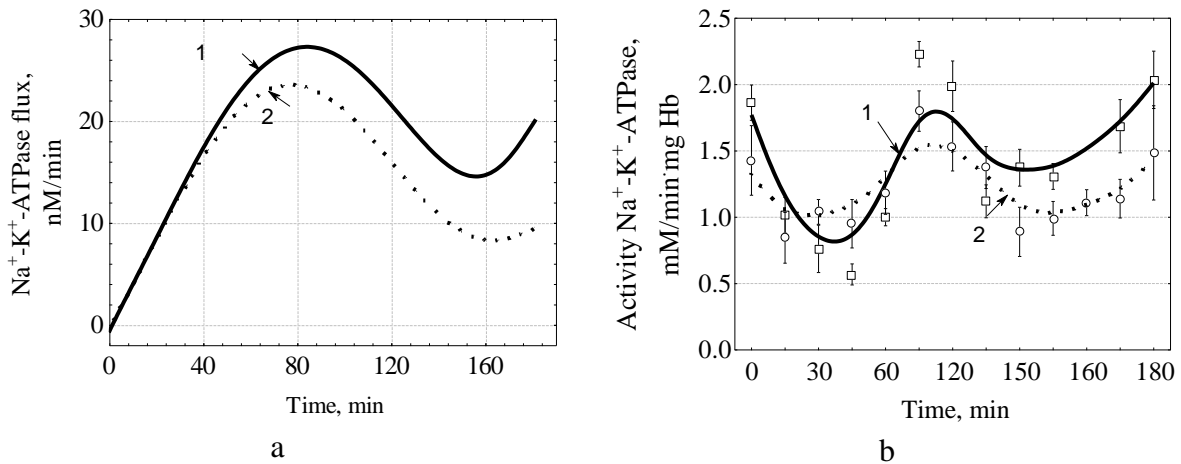

Fig. 4. Fluxes through Na^+, K^+-dependent ATPase obtained during simulation (a). Experimental dependences of Na^+, K^+-ATPase activity (b). 1 — Ca^{2+} is absent, 2 — 2 mM Ca^{2+} in the incubation medium

Based on the information about the inactivation of Na^+K^+-ATPase by high concentrations of intracellular Ca^{2+}, the kinetic equation for Na^+K^+-ATPase was modified (Equation 19, Research Materials and Methods). In the model, we use the inactivation constant (K_I) for Ca^{2+} ions equals 0.398 μM.

According to literature [25], K_I is within 1–10 μM. According to [25], at least part of the inhibitory effects of the internal calcium of Na^+K^+-ATPase is secondary to calcium-induced changes in the level of ATP in the cell, which arise because of Ca^{2+}-ATPase-mediated ATP hydrolysis, which exceeds, at least temporarily, the rate of glycolytic production of ATP. In

this model, we believe that the level of ATP in erythrocytes does not depend on Ca in the incubation medium. It is known that the activation of PMCA leads to a rapid depletion of ATP [11], so this effect is compensated by a smaller value of K_I.

The mechanism of Ca^{2+} ion extrusion is mediated by Ca^{2+}-ATPase (PMCA). The presence of the B-splice isoform of PMCA1 was shown for the membrane of human erythrocytes [40]. The latter contains a Ca^{2+}-calmodulin-binding domain, phosphorylation sites and a PDZ-binding domain, which is a docking terminal for a number of proteins [40]. An increase in intracellular free Ca^{2+} is sensed by PMCA and occurs in response to the interaction of the Ca^{2+} calmodulin complex with the C-terminus of the enzyme. In Ca^{2+}-loaded erythrocytes, the limiting factor of PMCA transport capacity is the availability of ATP.

The activity of Ca^{2+}-ATPases (Fig. 5) significantly depends on Ca^{2+}. According to the simulation results, the flux through this enzyme is an order of magnitude lower in the absence of Ca^{2+} (Fig. 5 a). In the absence of Ca^{2+}, an increase in flux (calculation) and enzyme activity (experiment, Fig. 5 b) is observed at the beginning of incubation. It is possible that Ca^{2+} ions appear in the cytosol due to a decrease in intracellular pH and increased dissociation of the Ca^{2+}-calmodulin complex.

In the presence of Ca^{2+}, we detect cooperative Ca^{2+} effects manifestations. Since the exact kinetic equation for Ca^{2+}-ATPase is unknown, we propose a kinetic equation that considers the literature data regarding the direct effect of Ca^{2+} on the enzyme (we increase the degree of cooperativity to 4). We also consider the cooperative effects of Ca^{2+} binding to calmodulin. This made it possible to obtain similar time dependences for the flux and activity of this enzyme. The decrease in Ca^{2+}-ATPase activity at the end of the experiment is associated with a decrease in ATP content.
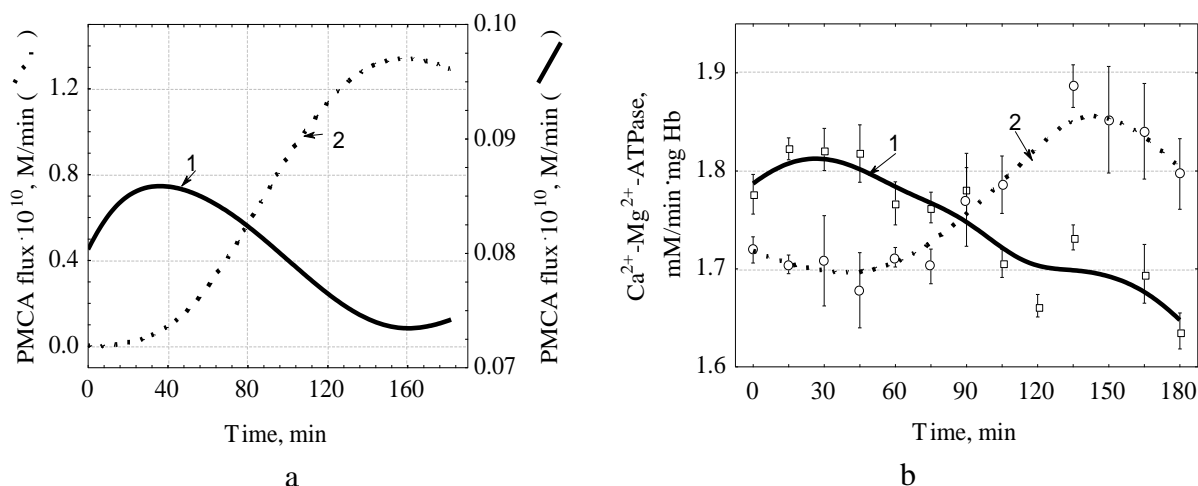

a   b

Fig. 5. Fluxes through Ca^{2+}-ATPase obtained during simulation (a). Experimental dependencies of Ca^{2+}-ATPase activity (b). 1 — Ca^{2+} is absent, 2 — 2 mM Ca^{2+} in the incubation medium.

Ionic homeostasis

The results of calculations of changes in the content of K^+, Na^+, Ca^{2+} and Cl^- in cells during incubation in saline solutions, in the absence (1) and presence (2) of Ca^{2+} ions are shown in Figure 6 a, b. Under the conditions of incubation in a medium without glucose and calcium (1), cells lose K^+ and Cl^- ions and increase the content of Na^+, but the influx of Na^+ ions is very small (0.4 mM after 3 hours of incubation). Incubation with Ca^{2+} increases the intracellular Ca^{2+} content due to a sudden increase in calcium permeability ($P_{Ca^{2+}}$) caused by a steep inward gradient. It is believed that the influx of Ca^{2+} occurs through an electrodiffusion conductive pathway [40, 41]. It is known that an increase in intracellular Ca^{2+} leads to

activation of Gardos channel (known as KCa3.1 or KCNN4 channels [42]) and outflux of K^+ from cells. The calculated flux through the Gardos channel for erythrocytes incubated in the presence of Ca^{2+} ions is shown in Figure 8 b. The outflux of K^+ ions occurs in parallel with the outflux of Cl^- and osmotically bound water. The result of these processes is a decrease in cell volume (Fig. 7 a). However, based on the simulation results, the content of K^+ ions in erythrocytes under conditions of Ca^{2+} activation remains higher than when the Gardos channel is not activated.
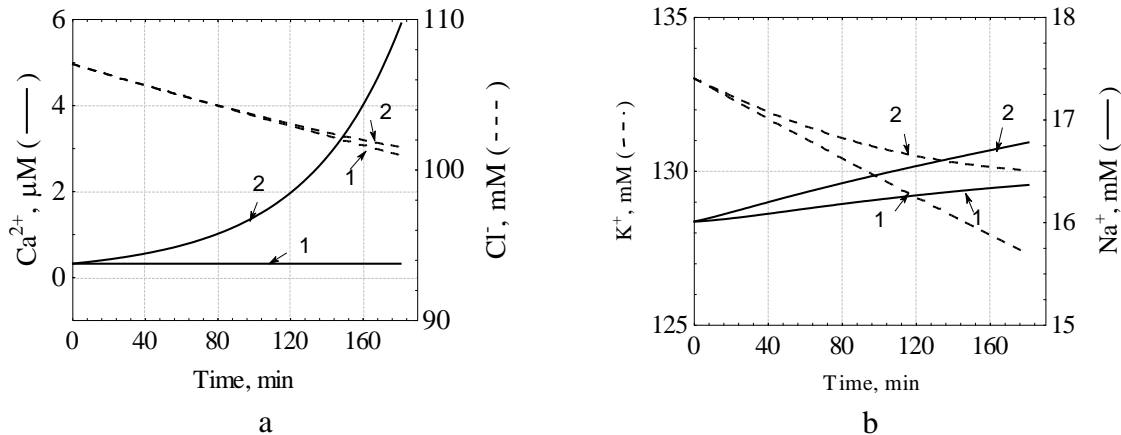

Fig. 6. Changes in the content of Ca^{2+} and Cl^- (a) and K^+, Na^+ (b) ions in erythrocytes during 3 hours of incubation in saline solutions in the absence (1) and presence (2) of Ca^{2+} ions.

According to the calculations, the activation of the Gardos channel leads to a decrease in the membrane potential (Fig. 7 a), which results in an increase in electrodiffusion fluxes into the cell, especially for Na^+ ions (Fig. 7 b). A significant part of passive ion fluxes occurs by the mechanism of electrodiffusion. Under physiological conditions, full experimental activation of Gardos channels induces a massive outward flux of K^+ and membrane hyperpolarization. A shift in the membrane potential creates a driving force for the extrusion of ions through conductive pathways. In this regard, the cell volume decreases equally during incubation without and in the presence of Ca^{2+} ions. Cell volume loss upon Gardos channel activation is largely limited by the rate of Cl^- efflux after K^+ efflux [41].

Na+, K+, 2Cl-, K+, Cl--cotransport

Na+, K+, 2Cl--cotransporter is a member of the cation-chloride cotransporter (CCC) superfamily. It moves one Na^+ ion, one K^+, and two Cl^- ions in one direction across the cell membrane in an electroneutral fashion. The operation of the transporter does not generate a current and changes in the transmembrane potential do not affect the flows mediated by the cotransporter [43]. A cotransporter can work in either direction, moving ions into or out of cells depending on chemical gradients. When the carrier is in equilibrium, the fraction: $[Na_{out}^+] \cdot [K_{out}^+] \cdot [Cl_{out}^-]^2 / [Na_{in}^+] \cdot [K_{in}^+] \cdot [Cl_{in}^-]^2 = 1$.

If the quotient is >1, activation of the transporter causes ions to enter the cell (positive flux value), and if it is <1, they leave of cell (negative flux value). The calculated flux through the Na^+, K^+, $2Cl^-$-transporter of erythrocytes incubated without Ca^{2+} and in the presence of Ca^{2+} ions are shown in Figure 8 a. Since the incubation medium did not contain K^+ ions, the flux of ions out of the cell takes place under the experimental conditions, which becomes slower over time. A negative correlation was shown between the maximum speed of cotransport and the potassium content in the cells, which indicates that the erythrocyte transporter can work in the efflux mode in vivo [43]. Activation of the Gardos channel by

Ca^{2+} ions (Fig. 8 b) creates an additional flux of K$^+$ from the cell, therefore, under these conditions, the flux through the Na$^+$, K$^+$, 2Cl$^-$-transporter reaches equilibrium faster (Fig. 8 a, dependence 2).
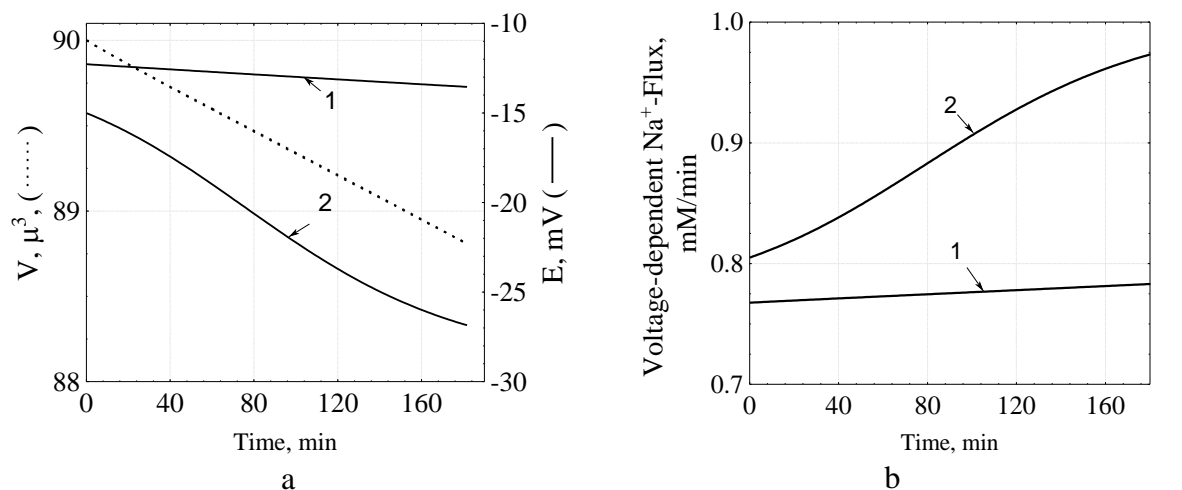

Fig. 7. Calculation of changes in volume (*V*) and membrane potential (*E*) of erythrocytes (a), electrodiffusion flux for Na$^+$ ions (b) during incubation in the absence (1) and presence (2) of Ca^{2+} ions.
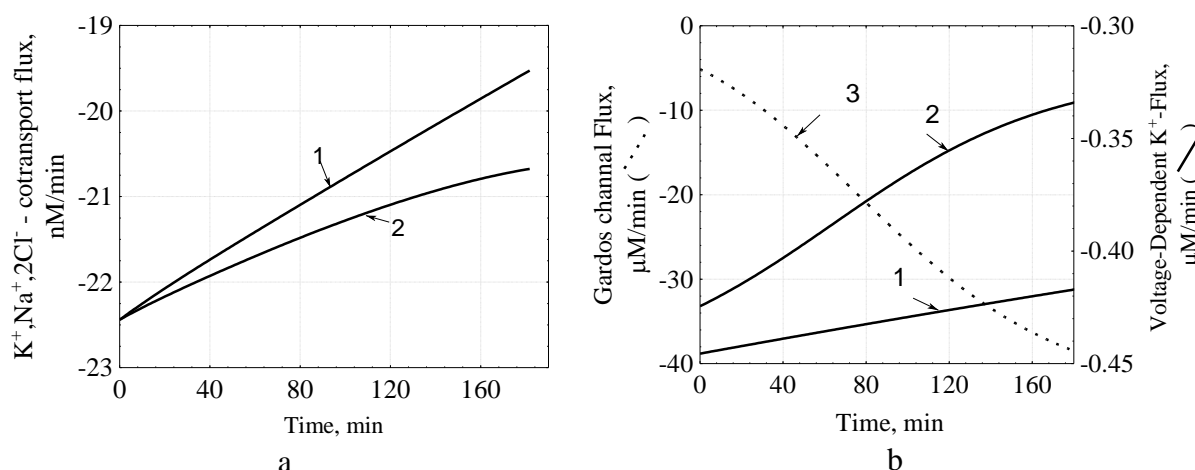

Fig. 8. The flux through the Na$^+$, K$^+$, 2Cl$^-$-cotransporter (a), electrodiffusion flux for K$^+$ ions (b) in erythrocytes during 3 hours of incubation in saline solutions in the absence (1) and presence (2) of ions Ca^{2+}. The flow through the Gardos channel (b, dependence 3) is modeled only for erythrocytes activated by Ca^{2+} ions.

Analysis of erythrocytes acid resistance

Next, we apply the simulation results to the analysis of acid resistance data of erythrocytes incubated in media of the same composition. The change in the time of the lag phase of hemolysis and the rate constant of hemolysis are shown in Fig. 9. According to experimental data, under the conditions of the presence of Ca^{2+} ions in the incubation medium, the time of the lag phase of hemolysis is reduced, but this reduction is reliably smaller compared to erythrocytes incubated in a medium without Ca^{2+}.

The entry of H$^+$ into the erythrocyte takes place with the participation of the Jacobs-Stewart cycle. The passage of H$^+$ through the anion exchanger is the limiting stage of hemolysis. Lysis of erythrocytes in an acidic environment is caused by denaturation and subsequent aggregation of membrane proteins [33]. As we show, during incubation, the volume of erythrocytes decreases, and the time of the lag phase is shortened compared to the

control, since for the same amount of transported H$^+$, their content in dehydrated cells will be higher. It is known that dehydrated cells have increased fragility and are more prone to hemolysis [4]. All the listed processes are the cause of both the reduction of the lag phase and the increase in the rate of hemolysis.
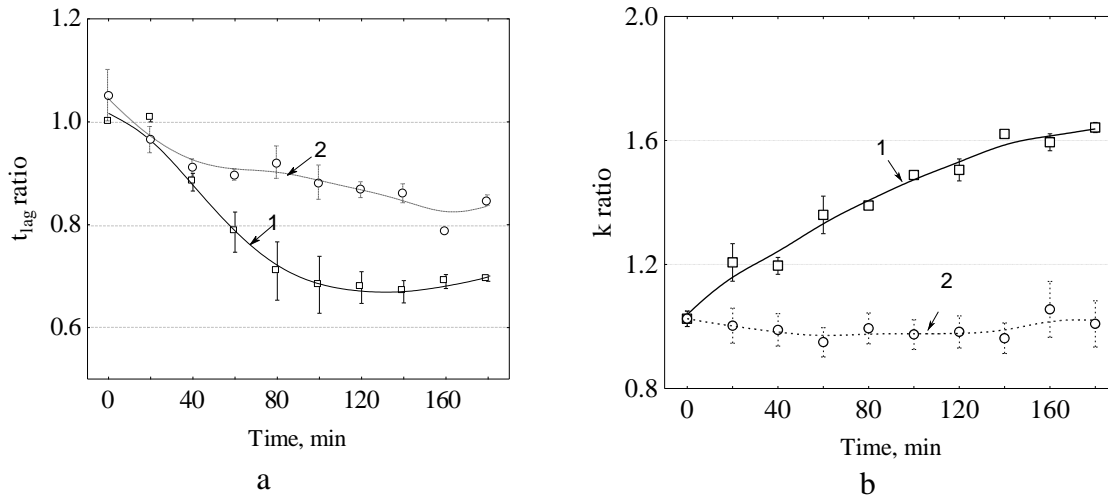

Fig. 9. Changes in the time of the lag phase of hemolysis (a) and the hemolysis rate constant (b) of erythrocytes during 3 hours of incubation in saline solutions, in the absence (1) and presence (2) of Ca^{2+} ions relative to the control level. Indicators in freshly isolated erythrocytes before the start of incubation were taken as the control level.

In erythrocytes incubated in the presence of Ca^{2+} ions, Ca^{2+}-ATPase is activated, intracellular pH decreases and Na$^+$/H$^+$ exchange is activated. High activity of the Na$^+$/H$^+$ exchanger can remove a certain amount of H$^+$ from the cell, which will reduce the efficiency of hemoglobin denaturation, and subsequently, less reduction of the lag phase is observed together with a decrease in the hemolysis rate constant.

However, it cannot be ignored that the effects of increasing the content of intracellular Ca^{2+} are more extensive. Increased intracellular Ca^{2+} activates Ca^{2+}-sensitive proteases, cross-linking of the cytoskeleton and formation of heme radicals. Therefore, Ca^{2+} homeostasis is an integrative function, and all processes regulating the content Ca_{in}^{2+} and their interactions must be taken into account when considering the activation of erythrocytes by Ca^{2+} ions.

CONCLUSIONS

The developed model is a tool for the quantitative analysis of the homeostasis of ions important for the regulation of intracellular pH and erythrocyte volume. The result of calculations based on the model are the time dependences of fluxes, concentrations of ions and metabolites, which allow to reproduction of the behavior of the metabolic system after disturbance in the conditions of the in vitro experiment and to establish the mechanisms of cell volume recovery.

We demonstrate that cation homeostasis in erythrocytes is primarily sustained by the active transport of Na$^+$ and K$^+$ through Na$^+$, K$^+$-ATPase, supplemented by comparatively lower passive permeability through alternative transport pathways. We show that with the presence of Ca^{2+} ions in the incubation medium and the activation of potassium release through Gardos channels, the cell volume is stabilized due to a change in the transmembrane potential and activation of electrodiffusion ion fluxes. We model the operation of the Na$^+$/H$^+$ exchanger and show its role in the presence of Ca^{2+}-ATPase activation. We show that a decrease in the acid resistance of erythrocytes during their incubation in a saline solution is

associated with a decrease in their cell volume and an increase in the acid resistance of erythrocytes during their incubation in the presence of Ca^{2+} ions is associated with the activation of the Na^+/H^+ exchanger.

CONFLICT OF INTEREST
The authors declare no conflicts of interest.

Authors' ORCID ID
O. I. Dotsenko ⓘhttps://orcid.org/0000-0003-3946-3515
G. V. Taradina ⓘhttps://orcid.org/0000-0001-8931-8370

REFERENCES
1. Ataullakhanov FI, Martinov MV, Shi Q, Vitvitsky VM. Significance of two transmembrane ion gradients for human erythrocyte volume stabilization. PLoS One. 2022 Dec 21;17(12):e0272675. https://doi.org/10.1371/journal.pone.0272675
2. Svetina S. Theoretical bases for the role of red blood cell shape in the regulation of its volume. Front Physiol. 2020 Jun 9;11:544. https://doi.org/10.3389/fphys.2020.00544
3. Glogowska E, Gallagher PG. Disorders of erythrocyte volume homeostasis. Int J Lab Hematol. 2015 May;37 Suppl 1:85–91. https://doi.org/10.1111/ijlh.12357
4. Gallagher PG. Disorders of erythrocyte hydration. Blood. 2017 Dec 21;130(25):2699–708. https://doi.org/10.1182/blood-2017-04-590810
5. Badens C, Guizouarn H. Advances in understanding the pathogenesis of the red cell volume disorders. Br J Haematol. 2016 Sep;174(5):674–85. https://doi.org/10.1111/bjh.14197
6. Flatt JF, Bruce LJ. The molecular basis for altered cation permeability in hereditary stomatocytic human red blood cells. Front Physiol. 2018;9:367. https://doi.org/10.3389/fphys.2018.00367
7. Shatrova A, Burova E, Pugovkina N, Domnina A, Nikolsky N, Marakhova I. Monovalent ions and stress-induced senescence in human mesenchymal endometrial stem/stromal cells. Sci Rep. 2022;12:11194. https://doi.org/10.1038/s41598-022-15490-2
8. Kaestner L, Bogdanova A, Egee S. Calcium channels and calcium-regulated channels in human red blood Cells. Adv Exp Med Biol. 2020;1131:625–48. https://doi.org/10.1007/978-3-030-12457-1_25
9. Fermo E, Bogdanova A, Petkova-Kirova P, Zaninoni A, Marcello AP, Makhro A, et al. 'Gardos Channelopathy': a variant of hereditary Stomatocytosis with complex molecular regulation. Sci Rep. 2017 May 11;7(1):1744. https://doi.org/10.1038/s41598-017-01591-w
10. Svetina S, Švelc Kebe T, Božič B. A model of Piezo1-based regulation of red blood cell volume. Biophys J. 2019 Jan 8;116(1):151–64. https://doi.org/10.1016/j.bpj.2018.11.3130
11. Ataullakhanov FI, Korunova NO, Spiridonov IS, Pivovarov IO, Kalyagina NV, Martinov MV. How erythrocyte volume is regulated, or what mathematical models can and cannot do for biology. Biochem. Moscow Suppl. Ser. 2009;A3:101–15. https://doi.org/10.1134/S1990747809020019
12. Brumen M, Heinrich R. A metabolic osmotic model of human erythrocytes. Biosystems. 1984;7(2):155–69. https://doi.org/10.1016/0303-2647(84)90006-6
13. Rogers S, Lew VL. PIEZO1 and the mechanism of the long circulatory longevity of human red blood cells. PLoS Comput Biol. 2021 Mar 10;17(3):e1008496. https://doi.org/10.1371/journal.pcbi.1008496
14. Lew VL. The circulatory dynamics of human red blood cell homeostasis: Oxy-deoxy and PIEZO1-triggered changes. Biophys J. 2023 Feb 7;122(3):484–495. https://doi.org/10.1016/j.bpj.2022.12.038
15. Yurinskaya VE, Moshkov AV, Marakhova II, Vereninov AA. Unidirectional fluxes of monovalent ions in human erythrocytes compared with lymphoid U937 cells: Transient processes after stopping the sodium pump and in response to osmotic challenge. PLoS One. 2023;18(5):e0285185. https://doi.org/10.1371/journal.pone.0285185
16. Dotsenko OI. The whole-cell kinetic metabolic model of the pH regulation mechanisms in human erythrocytes. Regul. Mech. Biosyst. 2022;13:272–80. https://doi.org/10.15421/022235
17. Mulquiney PJ., Kuchel PW. Model of 2,3-bisphosphoglycerate metabolism in the human erythrocyte based on detailed enzyme kinetic equations: equations and parameter refinement. Biochem J. 1999 Sep 15;342(3):581–96. https://doi.org/10.1042/bj3420581
18. Nishino T, Yachie-Kinoshita A, Hirayama A, Soga T, Suematsu M, Tomita M. Dynamic simulation and metabolome analysis of long-term erythrocyte storage in adenine-guanosine solution. PLoS One. 2013 Aug 16;8(8):e71060. https://doi.org/10.1371/journal.pone.0071060

19. Yastrebova ES, Konokhova AI, Strokotov DI, Karpenko AA, Maltsev VP, Chernyshev AV. Proposed Dynamics of CDB3 Activation in Human Erythrocytes by Nifedipine Studied with Scanning Flow Cytometry. Cytometry A. 2019 Dec;95(12):1275−84. https://doi.org/10.1002/cyto.a.23918

20. Pontremoli R, Zerbini G, Rivera A, Canessa M. Insulin activation of red blood cell Na^+/H^+ exchange decreases the affinity of sodium sites. Kidney Int. 1994 Aug;46(2):365−75. https://doi.org/10.1038/ki.1994.283

21. Semplicini A, Spalvins A, Canessa M. Kinetics and stoichiometry of the human red cell Na^+/H^+ exchanger. J Membr Biol. 1989 Mar;107(3):219−28. https://doi.org/10.1007/BF01871937

22. Bazanovas AN, Evstifeev AI, Khaiboullina SF, Sadreev II, Skorinkin AI, Kotov NV. Erythrocyte: A systems model of the control of aggregation and deformability. Biosystems. 2015 May;131:1−8. https://doi.org/10.1016/j.biosystems.2015.03.003

23. Martinov MV, Vitvitsky VM, Ataullakhanov FI. Volume stabilization in human erythrocytes: combined effects of Ca^{2+}-dependent potassium channels and adenylate metabolism. Biophys Chem. 1999 Aug 30;80(3):199−215. https://doi.org/10.1016/s0301-4622(99)00079-4

24. Yang YC, Yingst DR. Effects of intracellular free Ca and rate of Ca influx on the Ca pump. Am J Physiol. 1989 Jun;256(6 Pt 1):C1138−44. https://doi.org/10.1152/ajpcell.1989.256.6.C1138

25. Brown AM, Lew VL. The effect of intracellular calcium on the sodium pump of human red cells. J Physiol. 1983 Oct;343:455−93. https://doi.org/10.1113/jphysiol.1983.sp014904

26. Dolan AT, Diamond SL. Systems modeling of Ca^{2+} homeostasis and mobilization in platelets mediated by IP3 and store-operated Ca^{2+} entry. Biophys J. 2014 May 6;106(9):2049−60. https://doi.org/10.1016/j.bpj.2014.03.028

27. Iida S, Potter JD. Calcium binding to calmodulin. Cooperativity of the calcium-binding sites. J Biochem. 1986 Jun;99(6):1765−72. https://doi.org/10.1093/oxfordjournals.jbchem.a135654

28. Dotsenko OI, Troshchynskaya YA. Role of AMP catabolism enzymes in the energetic status of erythrocytes under conditions of glucose depletion. Biosystems Diversity. 2014;22(1):46−52. (In Russian). https://doi.org/10.15421/011406

29. Mendes P, Hoops S, Sahle S, Gauges R, Dada J, Kummer U. Computational modeling of biochemical networks using COPASI. Methods Mol Biol. 2009;500:17−59. https://doi.org/10.1007/978-1-59745-525-1_2

30. Dotsenko OI, Mykutska IV, Taradina GV, Boiarska ZO. Potential role of cytoplasmic protein binding to erythrocyte membrane in counteracting oxidative and metabolic stress. Regulatory Mechanisms in Biosystems. 2020;11(3):455–62. https://doi.org/10.15421/022070

31. Dotsenko OI, Mischenko AM, Taradina GV. Vibration influence on the O_2-dependent processes activity in human erythrocytes. Regulatory Mechanisms in Biosystems. 2021;12(3):452−8. https://doi.org/10.15421/022162

32. Dotsenko OI, Taradina GV, Mischenko AM. Peroxidase activity of erythrocytes hemoglobin under action of low-frequency vibration. Studia Biologica. 2021;15(4):3–16. https://doi.org/10.30970/sbi.1504.666

33. Dotsenko OI, Mischenko A.M. Influence of low-frequency vibration on the erythrocytes acid resistance. Biosystems Diversity. 2011;19(1):22−30 (In Russian). https://doi.org/10.15421/011104

34. Kherd AA, Helmi N, Balamash KS, Kumosani TA, Al-Ghamdi SA, Qari M, et al. Changes in erythrocyte ATPase activity under different pathological conditions. Afr Health Sci. 2017 Dec;17(4):1204−10. https://doi.org/10.4314/ahs.v17i4.31

35. Nikinmaa M. Gas transport. In: Bernhardt I, Ellory JC, editors. Red cell membrane transport in health and disease. Berlin, Germany: Springer; 2003. p. 489–509. https://doi.org/10.1007/978-3-662-05181-8

36. Geers C, Gros G. Carbon dioxide transport and carbonic anhydrase in blood and muscle. Physiol Rev. 2000 Apr;80(2):681−715. https://doi.org/10.1152/physrev.2000.80.2.681

37. Ugurel E, Goksel E, Cilek N, Kaga E, Yalcin O. Proteomic analysis of the role of the adenylyl cyclase-camp pathway in red blood cell mechanical responses. Cells. 2022 Apr 6;11(7):1250. https://doi.org/10.3390/cells11071250

38. Chi Y, Mo S, Mota de Freitas D. Na^+-H^+ and Na^+-Li^+ exchange are mediated by the same membrane transport protein in human red blood cells: an NMR investigation. Biochemistry. 1996 Sep 24;35(38):12433−42. https://doi.org/10.1021/bi9608141

39. Chu H, Puchulu-Campanella E, Galan JA, Tao WA, Low PS, Hoffman JF. Identification of cytoskeletal elements enclosing the ATP pools that fuel human red blood cell membrane cation pumps. Proc Natl Acad Sci USA. 2012 Jul 31;109(31):12794−9. https://doi.org/10.1073/pnas.1209014109

40. Bogdanova A, Makhro A, Wang J, Lipp P, Kaestner L. Calcium in red blood cells – A perilous balance. Int J Mol Sci. 2013;14(5):9848-9872. https://doi.org/10.3390/ijms14059848

41. Thomas SL, Bouyer G, Cueff A, Egée S, Glogowska E, Ollivaux C. Ion channels in human red blood cell membrane: Actors or relics? Blood Cells Mol Dis. 2011 Apr 15;46(4):261−5. https://doi.org/10.1016/j.bcmd.2011.02.007
42. Föller M, Lang F. Ion transport in eryptosis, the suicidal death of erythrocytes. Front Cell Dev Biol. 2020 Jul 8;8:597. https://doi.org/10.3389/fcell.2020.00597
43. Flatman PW. Regulation of Na-K-2Cl cotransport in red cells. In: Lauf PK, Adragna NC, editors. Cell Volume and Signaling. Advances in Experimental Medicine and Biology, vol 559. Springer, Boston, MA; 2004. P. 77−88. https://doi.org/10.1007/0-387-23752-6_7

ІОННИЙ ГОМЕОСТАЗ В РЕГУЛЮВАННІ ВНУТРІШНЬОКЛІТИННОГО pH ТА ОБ'ЄМУ ЕРИТРОЦИТІВ ЛЮДИНИ

О. І. Доценко*, Г. В. Тарадіна

Донецький національний університет імені Василя Стуса, вул. 600-річчя, 21, Вінниця, 21021, Україна
e-mail: o.dotsenko@donnu.edu.ua

Актуальність. Підтримка клітинного об'єму шляхом регулювання вмісту води та іонів має вирішальне значення для виживання і функціональної повноцінності еритроцитів людини. Разом з тим, клітини є неймовірно складними системами з численними, часто конкуруючими реакціями, що відбуваються одночасно. Тому, прогнозувати загальну поведінку системи або отримати нове розуміння того, як взаємодіють підкомпоненти системи, достатньо складно без застосування методів математичного моделювання.

Мета роботи. Створення математичної метаболічної моделі іонного гомеостазу еритроцитів для дослідження механізмів стабілізації об'єму еритроцитів і внутрішньоклітинного pH в експериментах *in vitro*.

Матеріали і методи. Математична модель створена з використанням загальних підходів до моделювання клітинного метаболізму, які базуються на системах звичайних диференціальних рівнянь, що описують метаболічні реакції, пасивні й активні потоки іонів. Для розробки моделі та розрахунків за моделлю використано середовище моделювання COPASI 4.38. Для перевірки моделі використовували зміни внутрішньоклітинного pH, активності Na^+/K^+-АТФази та Ca^{2+}-АТФази еритроцитів донора, інкубованих у сольових розчинах за відсутності та присутності іонів Ca^{2+}.

Результати. Створена кінетична модель іонного гомеостазу еритроцитів. З використанням реалістичних параметрів системи розраховані зміни у часі об'єму клітини, концентрацій і потоків метаболітів та іонів, трансмембранного потенціалу. Результати моделювання використані для аналізу причин змінення стійкості до кислотного гемолізу еритроцитів за умов їх інкубування у сольових розчинах різного складу.

Висновки. Ми показуємо, що катіонний гомеостаз в еритроцитах підтримується в основному активним рухом Na^+ і K^+ через Na^+, K^+-АТРазу у поєднанні з відносно нижчою пасивною проникністю через інші транспортні шляхи. За присутності іонів Ca^{2+} і активації виходу калію через Гардос-канали, об'єм клітин стабілізується за рахунок змінення трансмембранного потенціалу і активації електродифузійних потоків іонів. Показано, що зниження кислотної резистентності еритроцитів при їх інкубуванні у сольовому розчині зв'язано зі зменшенням об'єму клітин, а підвищення кислотної резистентності клітин при їх інкубуванні в присутності іонів Ca^{2+} — з активацією Na^+/H^+-обмінника.

КЛЮЧОВІ СЛОВА: математичне метаболічне моделювання; транспорт іонів; осмотичні процеси; електрохімічний мембранний потенціал; проникність іонів; Na^+/K^+-ATPase; Ca^{2+}-ATPase; кальмодулін; білок смуги 3 (AE1); Гардос-канали.